Copyright © 1998, by the International Council of the Aeronautical Sciences (ICAS)
and the American Institute of Aeronautics and Astronautics, Inc.

A98-31592

ICAS-98-4,5,1

Dynamic Load Development and Results for Dynamic Excitation of a Full-Scale F/A-18 Fatigue Test Article

D.P. Conser, C. Mouser and W. Waldman
Aeronautical and Maritime Research Laboratory
506 Lorimer St, Fishermens Bend
Melbourne, Victoria 3207, Australia

ABSTRACT

A unique technique has been developed to apply flight representative buffet dynamic loads to a full-scale F/A-18 fatigue test article while simultaneously applying manoeuvre loads. The simultaneous application of dynamic and manoeuvre loading is required to simulate the fatigue critical in-flight loading experienced during high angle of attack flying. Buffet dynamic loads are applied using a multi-channel, high force, high displacement electromagnetic shaker and control system. The approaches used to develop and apply the dynamic loading spectrum are discussed, with focus given to the development of the target flight-derived test article dynamic response and their comparison to test results.

1. Introduction

Although significant full-scale testing of the F/A-18 structure was conducted by the manufacturer to meet United States Navy design requirements, Australia and Canada have embarked upon a collaborative full-scale structural testing program, the F/A-18 International Follow On Structural Test Project (IFOSTP). The aim of IFOSTP is to determine the economic and safe life of the F/A-18 structure under loading that is more representative of Royal Australian Air Force (RAAF) and Canadian Forces (CF) operating conditions. Testing is being shared between the two countries. Canada is testing the centre fuselage and wings and Australia is testing the aft fuselage and empennage. The Australian portion of the test is being conducted at the Defence Science and Technology Organisation's Aeronautical and Maritime Research Laboratory (AMRL) in Melbourne, Australia.

A unique full-scale fatigue test system has been developed by AMRL which combines buffet induced dynamic loading with manoeuvre loading to simulate the flight loading conditions experienced by an F/A-18 aircraft under typical operations (Reference 1). The system uses a pneumatic loading system to apply the distributed aerodynamic and inertial loads induced by aircraft manoeuvres. The severe buffet dynamic loading experienced in flight is applied by high powered, high displacement electromagnetic shakers. This paper describes the AMRL test methodology and the approaches used to develop and apply the dynamic loading spectrum, concentrating on the development of the target flight-derived test article dynamic response and comparison to fatigue test results.

2. F/A-18 Operational Environment

The F/A-18 is an extremely manoeuvrable, high performance fighter/attack aircraft. The inner wing leading edge extension (LEX) provides lift enabling it to achieve angles of attack (AOA) in excess of 60°. The twin vertical tails canted slightly outward exploit the high-energy vortices generated by each LEX to provide directional stability at these high AOA conditions. However, these vortices break down at high AOA, buffeting the structure and exciting the resonance frequencies of the empennage, producing high acceleration levels at the tips of each vertical tail and horizontal stabilator. This empennage response excites engine and other aft fuselage resonant dynamic responses causing high dynamic stress levels in various structural components.

Due to the high dynamic response experienced by the empennage and aft fuselage, various structural modifications have been made to the airframe, including an aerodynamic modification known as the LEX fence. The LEX fence (Figure 1) was designed by the McDonnell Aircraft Company, referred to here as MDA, to alter the LEX vortex flow, reduce dynamic response levels and decrease airframe fatigue damage (Reference 2). Due to the dramatic change in the buffet dynamic loading with and without the LEX fence installed (Reference 3), loading spectra were derived for both the pre-LEX fence and post-LEX fence flight environments.

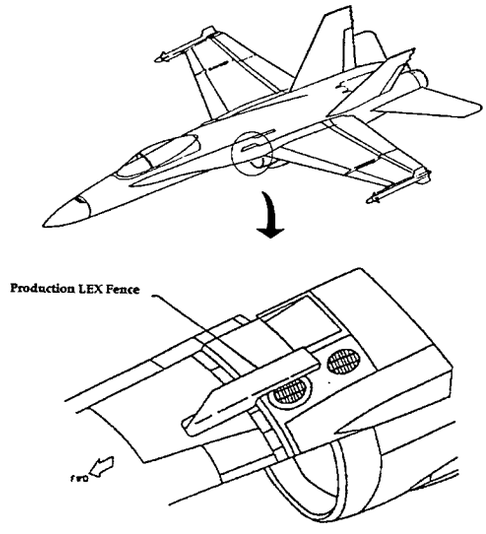

Figure 1 – F/A-18 LEX fence.

21st ICAS Congress
13-18 September 1998
Melbourne, Australia

Copyright © 1998 by ICAS and AIAA. All rights reserved

Copyright © 1998, by the International Council of the Aeronautical Sciences (ICAS)
and the American Institute of Aeronautics and Astronautics, Inc.

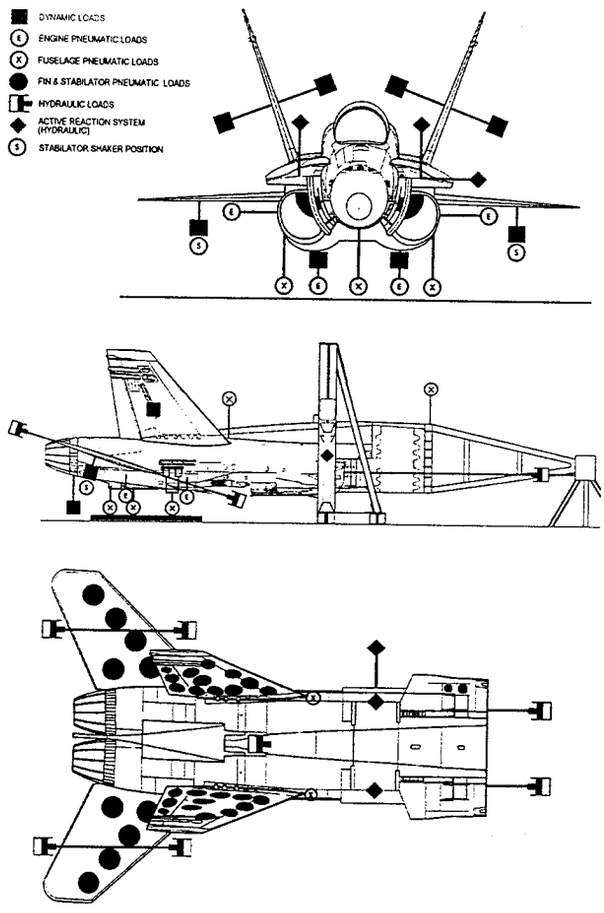

Figure 2 – IFOSTP FT46 actuator configuration.

This paper focuses on the development of the pre-LEX fence target dynamic loads and the test results obtained from pre-LEX fence testing.

3. IFOSTP Aft Fuselage General Testing Approach

The approach adopted for the AMRL test were dictated by the requirement to apply realistic buffet loads to the test article while simultaneously applying manoeuvre loading. This was required as dynamic loading is responsible for a large percentage of the fatigue damage caused in the F/A-18 aft fuselage and empennage structure. The simultaneous application of dynamic and manoeuvre loads was necessary as significant manoeuvre loading does occur while the structure is subjected to high buffet dynamic loading.

The primary objective of the loading development process was to load the test article in a manner such that its dynamic response matched as closely as possible that of an aircraft in flight. To accomplish this, a manoeuvre loading system was required that would not add significant mass, stiffness or damping to the structure as this would affect the dynamic characteristics of the structure.

Consequently, AMRL devised a loading system which would allow the critical structural modes of the empennage and engines to be excited under conditions comparable to flight, while still allowing the application of manoeuvre loads. This had the added benefit that the high number of dynamic load cycles could be applied more quickly than they have been in previous tests using conventional loading systems and equivalent static loads. The system developed to meet these IFOSTP requirements consists primarily of dual pneumatic soft springs to apply manoeuvre loads and electromagnetic shaker systems to impart the dynamic loads.

The IFOSTP F/A-18 test article, designated FT46, consists of the empennage surfaces and the centre and aft fuselage sections with a dummy forward fuselage spliced onto it. The nose of the forward fuselage is supported on a tripod and the test article is suspended from a heavy portal frame via hydraulic actuators connected at the wing attachment points of the centre fuselage. A spherical bearing at the fuselage nose allows the test article to rotate and bend but not translate. Scrap F/A-18 engines, dynamically similar to fleet engines, are installed in the test article in an attempt to ensure that the correct dynamic and manoeuvre loads are imparted into the engine mounts and support structure.

A large cathedral style reaction frame has been built for the vertical tail and stabilator manoeuvre loading actuators. A separate portal frame has been built to support the vertical tail dynamic shaker systems while the stabilator shaker systems are isolated and attached to the laboratory strong floor. A schematic of the test article and actuator system locations are shown in Figure 2.

The pre-LEX fence usage spectrum was developed from F/A-18 fleet usage data collected by the F/A-18 on-board data recording system. From this data, a mix of 250 flights was chosen to represent typical RAAF and CF F/A-18 fleet usage prior to the installation of the LEX fence. This sequence is termed SPEC6GE (Reference 4). Dynamic loads were then developed based on the high angle of attack flying (i.e. AOA>10°) present in these 250 flights using flight test data that were gathered specifically to define the empennage buffet environment.

4. Dynamic Loading Test Approach

The IFOSTP F/A-18 aft fuselage dynamic test approach objective is to apply representative dynamic loading to the test article. The dynamic excitation of the structure is applied by electromagnetic shakers using narrowband random excitation, with a constant power spectral density (PSD) level across the frequency bandwidth, and a form of input force control. This method is intended to allow for shifting structural resonances caused by structural non-linearities, manoeuvre loading system effects or changes which may occur as the airframe ages. Excitation is

Copyright © 1998, by the International Council of the Aeronautical Sciences (ICAS)
and the American Institute of Aeronautics and Astronautics, Inc.

Table 1 – F/A-18 vibration modes included in test.

Mode description	Approximate frequency (Hz)
Vertical tail 1st bending	16
Vertical tail 1st torsion	45
Stabilator 1st bending	12
Stabilator 2nd bending	38
Stabilator 1st torsion	46
Engine yaw	13
Engine pitch	14
Engine roll	38
Engine 1st lateral bending	44
Engine 1st vertical bending	49

simultaneously applied in the 10–20 Hz and 34–52 Hz bandwidths. Energy is applied at these frequencies to excite the resonant response shown to be critical to empennage and aft fuselage structural fatigue. The modes to be included in the AMRL IFOSTP fatigue test are listed in Table 1.

The level to which each mode is excited is defined based on response measurements obtained during F/A-18 flight testing. This response is characterised as a function of AOA and Q (dynamic pressure) as discussed in Section 5.2. The dynamic response of the structure is derived at key locations referred to as control accelerometers or control locations. These locations, shown in Figure 3, correspond to accelerometer locations used during F/A-18 flight testing where high dynamic response for a given surface or structure has been measured. The premise is that exciting the primary structural modes to match the flight response levels measured at these locations will result in the correct internal dynamic loading of the structure.

The electromagnetic shakers used to dynamically excite the test article have a four inch peak-to-peak stroke, a maximum force capacity of 5000 lbs and each is driven by a 65 kW amplifier. The shakers were built specifically for the test by LING Corp., USA. Shaker locations were selected that would allow excitation of all modes of interest in the 5–100 Hz frequency range, as initially it was thought it might be necessary to excite higher-order modes than those ultimately required. Load bridges are installed on each shaker attachment sting to permit measurement of the applied dynamic force.

A total of six shaker systems, comprised of eight individual shakers, may be used during testing. Two shakers are attached to each vertical tail and work together in a push-pull configuration. Their location optimises the dynamic excitation of the vertical tail modes. One shaker is attached to the lower surface of each horizontal stabilator. An additional shaker has been installed beneath each engine at the aft ring of the afterburner. These engine shakers are

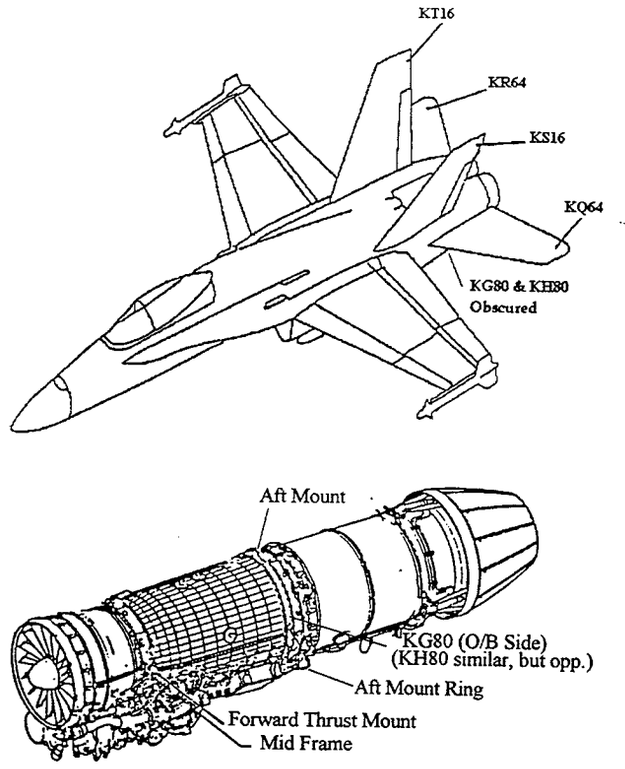

Figure 3 – F/A-18 IFOSTP control accelerometer locations.

aligned vertically to supplement excitation of the critical engine mount vertical dynamic loads. The engine shakers will only be used if excitation from the vertical tails and horizontal stabilators does not induce the correct dynamic loading in the engine mounts and backup structure. The requirement to add the engine shakers is being studied based on pre-LEX fence dynamic response test data obtained thus far and test data to be acquired during post-LEX fence testing which will utilise a different stabilator shaker attachment location.

Thus, the results discussed herein were obtained based on using only the six shakers during pre-LEX fence testing: two on each vertical tail and one on each stabilator. In addition, because only these four shaker systems were used, only the four empennage control accelerometers were used for pre-LEX fence test spectrum development. Approximate shaker locations are illustrated in Figure 2.

Modal survey tests were conducted to assess the resonance modes of the test article. Tests were conducted without the manoeuvre loading system active and then with the loading system active to assess the pneumatic and hydraulic actuators effect on resonance frequencies and mode shapes. Adjustments were made to the structure in some instances by strategically adding mass to the empennage surfaces to account for slight increases in some of the resonance frequencies under loading conditions. Dynamic strain

Copyright © 1998, by the International Council of the Aeronautical Sciences (ICAS)
and the American Institute of Aeronautics and Astronautics, Inc.

Table 2 – FT46 dynamic load validation channels.

Channel Designation	Location
20009 (LS42)	Port vertical tail FS557 stub
20010 (LT46)	Stbd vertical tail FS557 stub
19013 (LS27)	Port vertical tail FS566 stub
18013 (LS37)	Port vertical tail FS574 stub
17013 (LS38)	Port vertical tail FS580 stub
16013 (LS34)	Port vertical tail FS590 stub
15015 (LS33)	Port vertical tail FS598 stub
15016 (LT26)	Stbd vertical tail FS598 stub
28011	Port stabilator boot strap fitting
28012	Stbd stabilator boot strap fitting
28013 (LS50)	Port stabilator spindle
28014 (LS51)	Stbd stabilator spindle
23001 (LS11)	Port FS557 upper outboard longeron
15057 (LS13)	Port FS598 frame
15059 (LS14)	Port FS598 frame
15061 (LS15)	Port FS598 frame
23067 (LG07)	Port aft engine hanger
23068 (LG46)	Stbd aft engine hanger
KS16	Port vertical tail aft tip
KS01	Port vertical tail fwd tip
KT16	Stbd vertical tail aft tip
KT01	Stbd vertical tail fwd tip
KQ64	Port stabilator aft tip
KQ70	Port stabilator fwd tip
KR64	Stbd stabilator aft tip
KR70	Stbd stabilator fwd tip
KG33	Fwd engine mount outboard long.
KG34/KH34	Fwd engine mount outboard lateral
KG35/KH35	Fwd engine mount outboard vert.
KG37	Fwd engine mount inboard vertical
KG61/KH61	Aft engine mount inboard lateral
KG80/KH80	Aft engine mount outboard vertical

Note: 1. (xxxx) designates flight test channel name.
2. xxx designates accelerometers. Others are strain gauges.

surveys were also conducted to compare dynamic strains and frequency response functions with flight results. These tests confirmed that the test article was acceptably dynamically similar to a fleet aircraft for the modes of interest. Thus, the excitation of the required modes to flight response levels as measured at the control accelerometers should produce representative internal dynamic loading of the structure.

The force required to excite the structure to target response levels is defined by a testing process referred to as input force characterisation. Results from this testing are combined with usage spectrum flight parameter data and control accelerometer flight response measurements to derive the required shaker excitation forces and drive signals. These shaker drive signals create the dynamic excitation required to produce dynamic response similar to flight results for the flight conditions defined in the usage spectrum.

Once the required dynamic input forces have been defined, they are reapplied in all subsequent test blocks as they are deemed to characterise the in-flight buffeting force of the LEX vortices. The initial approach is to allow test article response to vary throughout testing as it presumably would through the life of the aircraft. In this sense, it is an input controlled test, although there is actually no feedback control on force. Rather, periodic amplifier, shaker, test article frequency response measurement tests are performed to correct the shaker drive signals for changes in the frequency response of the system to ensure that the same dynamic forces are applied throughout testing.

As the dynamic loading is applied to the test article, measurements acquired using a high speed data acquisition system are analysed to ensure dynamic loads applied are acceptable. These assessments are first made for the control accelerometers as the dynamic excitation was developed in an attempt to match response at these locations. In addition to the control accelerometers, assessments are made at other structural locations known as Dynamic Load Validation Channels (DLVCs). These locations were selected to cover major structural locations for which flight test measurements were available. The DLVCs, which are listed in Table 2, were chosen to assist in assessing the integrity of the dynamic loading method. Based on dynamic loading and fatigue assessments at these locations, adjustments to the dynamic loading are made if appropriate, possible and feasible.

While this section summarises the dynamic loading test approach, Reference 1 provides a more comprehensive description of the dynamic load spectrum development method, as well as additional information on the test loading systems, usage spectra analyses, etc.

5. Pre-LEX Fence Flight Tests

The buffet response on the vertical tails and horizontal tails of the F/A-18 becomes significant when the aircraft AOA exceeds about 10°. The 10–20 Hz and 32–52 Hz frequency bands show a significant modal response, and the rms (root-mean-square) response level in a given frequency band is a function of both AOA and Q. The dynamic response in these two frequency bands is commonly referred to as Mode 1 and Mode 2, respectively. There is also a broad-band response in the 80–100 Hz region under some AOA-Q conditions, but this is considered insignificant in terms of fatigue. The Mode 1 response on the vertical and horizontal tails is the primary bending mode of these two structures. The Mode 2 response on the vertical tails is described as a torsion mode, while on the horizontal tails the mode shape is a combination of bending and torsion.

5.1 Buffet response flight test measurements

In order to measure typical buffet-induced dynamic vibration responses that occur on the vertical tails,

Copyright © 1998, by the International Council of the Aeronautical Sciences (ICAS)
and the American Institute of Aeronautics and Astronautics, Inc.

horizontal tails, engine mounts, and other aft fuselage locations, two flight test programs were held in Canada by AETE (Aerospace Engineering Test Establishment) in 1989 and 1993. These were identified as PD 88/12 (Reference 5) and PD 93/03 (Reference 6), respectively, and both of these trials included flights with the LEX fences off and on. The measurands consisted of accelerometer and strain gauge channels corresponding to those listed in Table 2, as well as other locations.

The PD 88/12 flight trials provided significant data quantifying the F/A-18 aft fuselage and empennage dynamic environment. However, insufficient or in some cases no data were acquired for some critical flight conditions. Thus, the objective of the PD 93/03 flight trials was to supplement the PD 88/12 data by gathering as much additional data as possible at high AOA and Q conditions that were at the extremes of the flight envelope, defined by the 250 flight usage spectra, where a significant buffet response was present. For example, the total time in the AOA-Q bin for the 28°–32° and 300–350 psf region from LEX fences off flying during PD 88/12 was only 9.2 seconds, and PD 93/03 provided an additional 35.2 seconds of data. This significantly increased the amount of available data for this buffet response region, and similar increases were obtained for other AOA-Q bins where previously only minimal amounts of data were present. Additional data were also obtained for many of the less extreme AOA-Q bins, which helped to enhance the overall quality of the database for the purpose of obtaining averaged power spectra within each specified AOA-Q bin.

Buffet response data were also obtained from flight trials undertaken by the RAAF Aircraft Research and Development Unit (ARDU) in Australia, as well as those conducted by MDA in the USA. Therefore, the total buffet response database consisted of four sets of different flight trials that were flown using three different F/A-18 aircraft.

5.2 AOA-Q matrix of flight conditions

The flight testing was carried out for flying that was representative of ACM (Air Combat Manoeuvre) training, as well as for specific PITS (Points In The Sky) covering a wide range of AOA and Q conditions that are representative of in-service operations. The severity of the vortex buffet pressures can be gauged from the fact that they are capable of producing a maximum peak-to-peak vibration amplitude of approximately 11 inches in Mode 1 at the tips of the vertical tails. Each of the four flight trials achieved a slightly different AOA-Q coverage and was carried out with varying measurands.

Because the buffet response is a function of both AOA and Q, the operational flight envelope of the F/A-18 was subdivided into a matrix of AOA-Q bins. This allowed general trends in the buffet response to be determined and important features to be identified (e.g. flight conditions where the greatest responses occurred). A small subset of the final AOA-Q matrix that was defined for analysing the measured buffet response data and presenting the results is shown in Table 3 for illustrative purposes.

Table 3 – Subset of typical AOA-Q matrix.

	Dynamic pressure Q (psf)				
Angle of attack (degrees)	75 to 125	125 to 175	175 to 225	225 to 300	300 to 350
8 – 12					
12 – 16					
16 – 20					
20 – 24					
24 – 28					

The complete coverage of the AOA-Q matrix achieved by the various flight test programs is such that it contains data suitable for use in replicating the buffet response environment encountered under RAAF and CF usage spectra. A description of the development of the F/A-18 usage spectrum for the IFOSTP fatigue test can be found in Reference 4.

During AETE flight testing, the PITS consisted of predefined manoeuvres where the test pilot was asked to try to maintain the target AOA and Q conditions for as long as possible. To make this a feasible task, the test point was defined to fall within a small range of AOA and Q around the nominated target conditions. Some of the PITS involved flying close to the limits of the F/A-18 flight envelope, and as a result those particular test points generally could not be sustained for any significant length of time. Under these circumstances the pilot was requested to attempt a minimum of three repeats to try and gather at least 20 seconds of data within the selected AOA-Q bin. In other flights, typical air combat manoeuvres were flown to provide data representative of squadron conditions.

In many cases the desired flight conditions were so difficult to achieve that only a few seconds of data could be acquired given even the best efforts of the pilot. In other instances, continuous on-condition data runs of more than 40 seconds could be easily achieved, so some AOA-Q bins accumulated larger amounts of data than others. Long data sequences were beneficial because signal averaging could be performed during the analysis to reduce the statistical variance in computed response parameters. In any case, whenever the more extreme manoeuvres were attempted there was a concomitant gathering of time spent in adjacent AOA-Q bins which often yielded usable data fragments.

In relation to the AOA-Q matrix shown in Table 3, there are a number of pertinent points that should be mentioned. One of these concerns the choice of the interval size

Copyright © 1998, by the International Council of the Aeronautical Sciences (ICAS)
and the American Institute of Aeronautics and Astronautics, Inc.

covered by the AOA bands. Although 4° steps in AOA are now being used, the original choice was to use 2° steps in order to obtain a better resolution when assessing trends in the buffet response. However, the use of 2° steps would have produced smaller time accumulations in each of the AOA-Q bins at the flight envelope extremes, leading to less statistically reliable estimates of the buffet response characteristics in those regions. Also, the number of AOA-Q bins for which buffet excitation sequences would need to be computed would be approximately doubled, leading to extra time being required for testing due to additional preparation work.

5.3 Processing of buffet response data

The buffet response that was measured during the flight trails was analysed in the frequency domain in order to ascertain its spectral characteristics. Autospectra, cross-spectra, coherence functions, and frequency response functions were computed at various stages of the analysis. Both Fortran and C software was custom written to carry out these analyses. The analyses were conducted over the full flight AOA-Q matrix.

Extensive time domain analyses were also conducted. These included preliminary data integrity checks using simple time series statistics such as rms response, minimum and maximum responses, and peak-to-rms response ratios. The validated data were then bandpass filtered into the Mode 1 and Mode 2 response regions using FIR digital filters (Reference 7). Peak-valley exceedences and rms responses were determined for all available bins in the AOA-Q matrix.

6. Pre-LEX Fence Dynamic Response Database

Before fatigue testing could commence, the available flight data was used to define target dynamic response levels for FT46, and thus define the internal dynamic loading of the structure. The first step in developing this target pre-LEX fence dynamic response database was to derive the rms responses required at the control accelerometers for all AOA-Q flight conditions covered by the test usage spectra.

The rms acceleration response was required for the two frequency bands to be tested, 10–20 Hz and 32–52 Hz, covering the modes of interest. It should be noted that while the second bandwidth used in flight test data processing is slightly different than the 34–52 Hz test bandwidth, the effect of this is insignificant as there is very little flight response between 32 Hz and 34 Hz. Thus, the test bandwidth was narrowed to prevent unnecessary energy from being applied to the test article.

Examination of the available flight test data indicated differences in the control accelerometer response magnitudes for the various flight test programs. In some cases, the difference was quite significant. Thus, choosing a single flight test program to derive the target dynamic response for FT46 would yield a dynamic loading spectra biased towards the severity of the program selected. Statistical examination of the flight test measurements indicated that the data samples, while from flight test aircraft with slightly different aft fuselage structural configurations, were from the same statistical data population. Thus, all available flight test data for the control accelerometers were used to define the target dynamic response for the fatigue test.

To accomplish this, the response measurements from all four flight test programs were combined on a time-weighted basis to produce an average target response in each AOA-Q region. The equation used to calculate the control accelerometer rms response for each AOA-Q region was:

$$A_j = \sum_{i=1}^{4} R_{ij} \frac{t_{ij}}{T_j}$$

where

i = index representing each of the four flight test programs (PD 88/12, PD 93/03, ARDU and MDA);

j = index representing the AOA-Q condition;

A_j = the time-weighted average rms response based on available data from all flight tests for the jth AOA-Q condition;

R_{ij} = rms response for the ith flight test program for the jth AOA-Q condition;

t_{ij} = time accumulation for ith flight test program for the jth AOA-Q condition;

T_j = total time accumulation from all flight test programs for the jth AOA-Q condition.

This time-weighted database (TWDB) of control accelerometer average rms responses was calculated for each AOA-Q region and was done for both the 10–20 Hz and 32–52 Hz frequency bandwidths. However, as a result of the differing AOA-Q coverage amongst the flight test programs, the final result for some AOA-Q regions was based on only one flight test program. These TWDB values were calculated separately for both right and left hand accelerometers (e.g. KS16 and KT16) for a given frequency band. The maximum rms acceleration measured on either the right or left side for a given surface was then chosen. This approach accounted for variations in response magnitudes across the aircraft and was adopted to yield a more conservative and symmetric dynamic loading spectrum.

Copyright © 1998, by the International Council of the Aeronautical Sciences (ICAS)
and the American Institute of Aeronautics and Astronautics, Inc.

Despite the amount of flight test data available, there were some regions where usage time existed but no flight test measurements were available. The rms response was predicted for these regions by extrapolation using a gradient approach based on TWDB rms response variations in adjacent AOA-Q regions. Predictions greater than the maximum TWDB rms for the respective accelerometer were set equal to the maximum TWDB rms. This prediction approach, while not sophisticated, was deemed appropriate as very little test time existed in AOA-Q regions requiring predictions.

The final TWDB result was a table of target pre-LEX fence rms response levels for each AOA-Q region, for each control accelerometer, for the 10–20 Hz and 32–52 Hz frequency bandwidths. The maximum target pre-LEX fence acceleration response for empennage control accelerometers is provided in Table 4.

The TWDB rms accelerations were integral to dynamic load spectrum development and test results could be compared to these results to ensure similar rms responses were measured during fatigue testing. However, while the rms might compare well, it is also important to assess the associated response distributions as the peak-valley or range pairs are critical when it comes to fatigue damage. However, because of the way the TWDB was developed, time history data were not available that had rms values matching the TWDB levels. Therefore, time history data measured during flight testing were scaled on a per AOA-Q basis to produce time histories with the desired TWDB rms response. For those bins missing data, time histories from adjacent bins were scaled to match the appropriate TWDB level. The response distributions from these scaled TWDB time histories were then used along with the test usage spectra to generate exceedence curves representing peak-valley exceedences expected for the 250 flight usage spectra if the TWDB rms response levels were obtained during testing. The TWDB rms tables and predicted exceedence curves are the targets against which test results were compared.

In addition to the control accelerometers, a TWDB was needed for the DLVC locations discussed previously. However, because most DLVCs were only available in one of the flight test programs, a similar approach of time weighting response measurements from all four flight programs could not be used. Thus, a process was developed to predict the rms response at the DLVC structural locations should the TWDB response levels be achieved at the control accelerometers. The method produced TWDB tables of rms response for the DLVCs. Exceedence curves were generated in a similar manner to those predicted for the control accelerometers. The technique that was used will be discussed in detail in Section 7. The TWDB rms and exceedence results discussed above will be presented when comparisons to test results are made in Section 8.

Table 4 – Maximum FT46 pre-LEX fence target control accelerometer response.

Empennage surface	Frequency bandwidth (Hz)	Maximum control acceleration (g rms)
Vertical Tail	10–20	37.1
	32–52	128.7
Horizontal Stabilator	10–20	22.6
	32–52	56.9

It is important to point out that due to some problems exciting stabilator modes in the 34–52 Hz bandwidth, the stabilator TWDB levels applied during pre-LEX fence testing were scaled to one third the levels resulting from the TWDB process. This was necessary as the stabilator 2nd bending and 1st torsion modes were not being excited in the correct proportion. In fact, excessive torsion loading was evident during the pre-test dynamic strain survey and thus, testing the stabilator to the flight TWDB control accelerometer levels would have over tested structure sensitive to stabilator torsion by a factor of approximately three. To avoid this, the test response levels were reduced.

The stabilator dynamic loading problem was assessed as being due to the stabilator shaker location near the stabilator trailing edge. While the shaker was ideally placed to excite the modes separately, it did not excite the modes with the correct combination at higher excitation levels. As a result, the shaker has been moved to a leading edge location for post-LEX fence testing. While any structural loading sensitive to stabilator response in this bandwidth was under tested for pre-LEX fence testing, this fact can be handled through analysis. This is possible because the post-LEX fence stabilator loading is basically unaffected by the LEX fence and thus the 5 blocks of pre-LEX fence loading represents a small percentage of the loading that the stabilator will experience during the remainder of the test.

7. Multiple-Input Frequency Response Functions

As mentioned earlier, not all of the DLVCs were monitored during all four flight test programs used to define the target FT46 pre-LEX fence control accelerometer response. Therefore, the same time-weighting process used in establishing the target control accelerometer response could not be used to define the target dynamic response expected at these locations. For these cases, multiple-input frequency response function analyses were performed on the available flight test data to define frequency response relationships between these locations and the four empennage control accelerometer locations (KS16, KT16, KQ64 and KR64). These relationships were then applied to

Copyright © 1998, by the International Council of the Aeronautical Sciences (ICAS)
and the American Institute of Aeronautics and Astronautics, Inc.

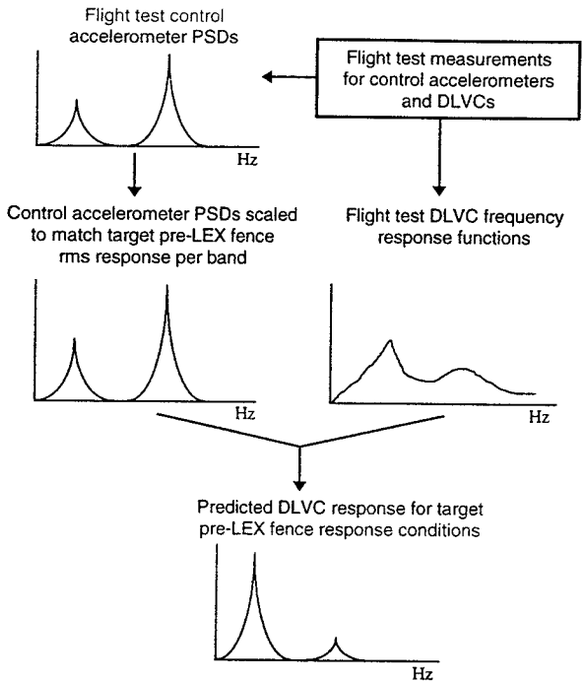

Figure 4 – DLVC response prediction for target control accelerometer response conditions.

flight spectra that were scaled to yield the target control channel rms levels per band. The result was PSDs of predicted response for all DLVCs per AOA-Q bin. A schematic of this process is shown Figure 4. In general, the response for all DLVCs could be predicted based on the four control channels that were used, with high coherence present in the frequency ranges of interest. The mathematical development of the theory of multiple-input frequency response analysis will now be described.

7.1 Basic multiple-input single-output relationships

Following closely the theory presented in Reference 8, consider q clearly defined measurable inputs $x_i(t)$, $i = 1, 2,\ldots, q$, which pass through q constant-parameter linear systems with frequency response functions $H_i(f)$, $i = 1, 2,\ldots, q$, so as to produce a single measured output $y(t)$, as illustrated in Figure 5. The output $y(t)$ will be the sum of the q ideal predicted linear outputs $v_i(t)$, $i = 1, 2,\ldots, q$, plus all possible deviations from the ideal model included in the unknown $n(t)$, as shown in Figure 5. $n(t)$ can include unknown extraneous components, if any, which may be present. Optimum choices of $H_i(f)$ in the least-squares sense will make $n(t)$ uncorrelated with $x_i(t)$. This situation is a realistic case where it is desired to estimate $H_i(f)$ and $n(t)$ from measurements of $x_i(t)$ and $y(t)$.

The governing equation for the output $y(t)$ in Figure 5 is

$$y(t) = \sum_{i=1}^{q} v_i(t) + n(t) \qquad (1)$$

where $v_i(t)$ is defined as that part of the output which is produced by the ith input when all the other inputs are zero.

The governing finite Fourier transform equations for the output $y(t)$ are

$$\begin{aligned} Y(f,T) &= \sum_{i=1}^{q} V_i(f,T) + N(f,T) \\ V_i(f,T) &= H_i(f) X_i(f,T) \quad i = 1,2,\ldots,q \end{aligned} \qquad (2)$$

where $Y(f,T)$, $V_i(f,T)$, $X_i(f,T)$ and $N(f,T)$ are the Fourier transforms of $y(t)$, $v_i(t)$, $x_i(t)$ and $n(t)$, respectively, computed over long sample records of length T. To simplify notation, all finite Fourier transforms will be denoted by capital letters without notation for their frequency and record-length dependence. Therefore, Equation (2) can be written as

$$Y = \sum_{i=1}^{q} V_i + N \qquad V_i = H_i X_i \qquad i = 1,2,\ldots,q \qquad (3)$$

To determine the basic input/output relationships, we start with Equation (3) and multiplying Y by Y^*, where the

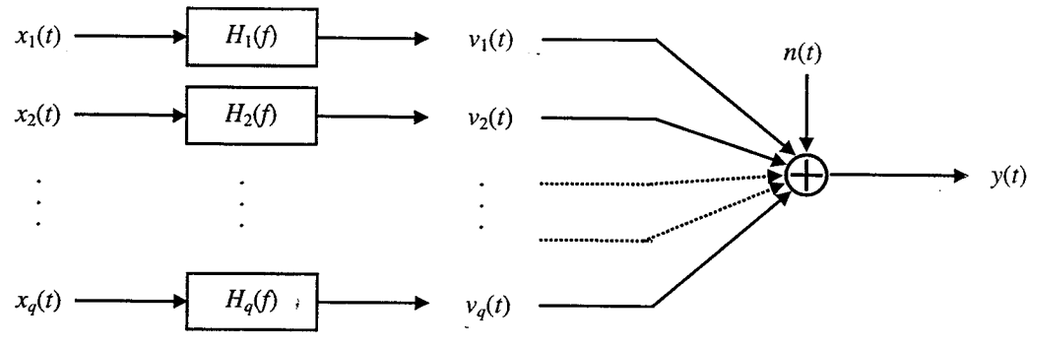

Figure 5 – Multiple-input single-output linear system.

Copyright © 1998, by the International Council of the Aeronautical Sciences (ICAS)
and the American Institute of Aeronautics and Astronautics, Inc.

symbol * denotes the complex conjugate, it follows that

$$Y^*Y = (\sum_{i=1}^{q} H_i X_i + N)^* (\sum_{j=1}^{q} H_j X_j + N)$$
$$= \sum_{i=1}^{q}\sum_{j=1}^{q} H_i^* H_j X_i^* X_j + N^*N +$$
$$\sum_{i=1}^{q} H_i^* X_i^* N + \sum_{j=1}^{q} H_j X_j N^*$$

When $n(t)$ and $x_i(t)$ are uncorrelated the last two terms in the last line of the above equation will average out to zero, and we obtain

$$Y^*Y = \sum_{i=1}^{q}\sum_{j=1}^{q} H_i^* H_j X_i^* X_j + N^*N \qquad (4)$$

Also, by multiplying the right hand side of Equation (3) by Y^* we obtain

$$Y^*Y = \sum_{i=1}^{q} H_i X_i Y^* + Y^*N \qquad (5)$$

Now, by taking the complex conjugate of both sides of Equation (5), and noting that $YY^* = Y^*Y$, we obtain

$$Y^*Y = \sum_{i=1}^{q} H_i^* X_i^* Y + N^*Y \qquad (6)$$

The two-sided cross-spectral density function between two random processes $x_i(t)$ and $y(t)$ is defined using X_i^*Y and not X_iY^* by

$$S_{x_i y} = \lim_{T\to\infty} \frac{1}{T} E\left[X_i^*(f,T)Y(f,T)\right] \qquad (7)$$

where the expected-value operator E denotes an averaging operation.

From the definition in Equation (7), taking expected values of Equation (4) and dividing by T yields, in the limit as T approaches infinity, the autospectrum of $y(t)$ as

$$S_{yy} = \sum_{i=1}^{q}\sum_{j=1}^{q} H_i^* H_j S_{ij} + S_{nn} \qquad (8)$$

Using Equation (6), this is equivalent to

$$S_{yy} = \sum_{i=1}^{q} H_i^* S_{iy} + S_{ny} \qquad (9)$$

Spectral quantities can be obtained here using a finite T as follows:

$$S_{yy} = \frac{E\left[Y^*Y\right]}{T} \qquad S_{ij} = \frac{E\left[X_i^*X_j\right]}{T}$$
$$S_{nn} = \frac{E\left[N^*N\right]}{T} \qquad S_{iy} = \frac{E\left[X_i^*Y\right]}{T} \qquad (10)$$
$$S_{ny} = \frac{E\left[N^*Y\right]}{T} \qquad S_{in} = \frac{E\left[X_i^*N\right]}{T}$$

Note that the quantity

$$S_{ny} = S_{nn} \quad \text{when } S_{in} = 0 \qquad (11)$$

Also, since $S_{yy}^* = S_{yy}$ and $S_{iy}^* = S_{yi}$, it follows that

$$S_{yy} = \sum_{i=1}^{q} H_i S_{yi} + S_{ny} \qquad (12)$$

Multiplication of Equation (3) by X_i^* after first changing the index of summation to j shows

$$X_i^*Y = \sum_{j=1}^{q} H_j X_i^* X_j + X_i^*N \qquad (13)$$

Expected values and divisions by T give

$$S_{iy} = \sum_{j=1}^{q} H_j S_{ij} \qquad i = 1,2,\ldots,q \qquad (14)$$

when $S_{in} = 0$. Equation (14) is a set of q equations that can be solved for the q unknown H_j when the model is well defined and when all of the $S_{iy}(f) = S_{x_i y}(f)$ and $S_{ij}(f) = S_{x_i x_j}(f)$ are known.

If it is assumed that the inputs are mutually uncorrelated and have zero means, then Equation (14) reduces to

$$S_{iy} = H_i S_{ii} \qquad i = 1,2,\ldots,q \qquad (15)$$

This shows that the overall system of Figure 5 is now merely a combination of simple single-input/single-output systems, where the frequency response function result indicates that the frequency response characteristics H_i of

Copyright © 1998, by the International Council of the Aeronautical Sciences (ICAS)
and the American Institute of Aeronautics and Astronautics, Inc.

the ith path associated with input $x_i(t)$ can be determined without regard to the other inputs that may be present. Of course, these other inputs affect the coherence function and the statistical accuracy in estimating H_i from measured data.

7.2 Matrix formulation of results

The preceding formulas can be expressed more concisely by the use of matrix notation (Reference 9). First, define a q-dimensional input vector

$$\mathbf{x}(t)=\begin{bmatrix} x_1(t) \\ \vdots \\ x_q(t) \end{bmatrix} \qquad (16)$$

Also, define a q-dimensional frequency response function vector

$$\mathbf{H}(f)=\begin{bmatrix} H_1(f) \\ \vdots \\ H_q(f) \end{bmatrix} \qquad (17)$$

Next, define a q-dimensional cross-spectrum vector of the output $y(t)$ with the inputs $x_i(t)$,

$$\mathbf{S}_{xy}(f)=\begin{bmatrix} S_{1y}(f) \\ \vdots \\ S_{qy}(f) \end{bmatrix} \qquad (18)$$

where

$$S_{iy}(f)=S_{x_iy}(f) \qquad (19)$$

and $S_{iy}(f)$ represents the cross-spectral density between the input $x_i(t)$ and the output $y(t)$.

Finally, define the $q\times q$ spectral matrix of all the inputs $x_i(t)$ by

$$\mathbf{S}_{xx}(f)=\begin{bmatrix} S_{11}(f) & S_{12}(f) & \cdots & S_{1q}(f) \\ S_{21}(f) & S_{22}(f) & \cdots & S_{2q}(f) \\ \vdots & \vdots & \ddots & \vdots \\ S_{q1}(f) & S_{q2}(f) & \cdots & S_{qq}(f) \end{bmatrix} \qquad (20)$$

where

$$S_{ij}(f)=S_{x_ix_j}(f) \qquad i,j=1,2,\ldots,q \qquad (21)$$

In Equation (21), $S_{ij}(f)$ represents the cross-spectral density function between the inputs $x_i(t)$ and $x_j(t)$.

The equation for computing the autospectrum of the response $y(t)$ in terms of the cross-spectra of the inputs and the frequency response functions may be written in matrix form as

$$S_{yy}(f)=\mathbf{H}^{*T}(f)\mathbf{S}_{xx}(f)\mathbf{H}(f) \qquad (22)$$

with the symbol ^{T} denoting the transpose. Note that $S_{yy}(f)$ in the above equation is still a scalar quantity but the other quantities are not. Note that the matrix $\mathbf{S}_{xx}(f)$ is Hermitian (meaning that $\mathbf{S}_{xx}(f)=\mathbf{S}_{xx}^{*T}(f)$).

When fully written out, Equation (22) becomes

$$S_{yy}(f)=\begin{bmatrix} H_1^*(f) & H_2^*(f) & \ldots & H_q^*(f) \end{bmatrix}\times \begin{bmatrix} S_{11}(f) & S_{12}(f) & \cdots & S_{1q}(f) \\ S_{21}(f) & S_{22}(f) & \cdots & S_{2q}(f) \\ \vdots & \vdots & \ddots & \vdots \\ S_{q1}(f) & S_{q2}(f) & \cdots & S_{qq}(f) \end{bmatrix}\begin{bmatrix} H_1(f) \\ H_2(f) \\ \vdots \\ H_q(f) \end{bmatrix} \qquad (23)$$

In the case of uncorrelated inputs the off-diagonal elements of matrix $\mathbf{S}_{xx}(f)$ become zero. It should be emphasised, however, that this result applies only to an ideal noise-free situation.

Using the previous definitions, the system of simultaneous equations given by Equation (14) may be written as a matrix equation

$$\mathbf{S}_{xy}(f)=\mathbf{S}_{xx}(f)\mathbf{H}(f) \qquad (24)$$

This is equivalent to

$$\begin{bmatrix} S_{1y}(f) \\ S_{2y}(f) \\ \vdots \\ S_{qy}(f) \end{bmatrix}=\begin{bmatrix} S_{11}(f) & S_{12}(f) & \cdots & S_{1q}(f) \\ S_{21}(f) & S_{22}(f) & \cdots & S_{2q}(f) \\ \vdots & \vdots & \ddots & \vdots \\ S_{q1}(f) & S_{q2}(f) & \cdots & S_{qq}(f) \end{bmatrix}\begin{bmatrix} H_1(f) \\ H_2(f) \\ \vdots \\ H_q(f) \end{bmatrix} \qquad (25)$$

The matrix equation can be solved for the column vector $\mathbf{H}(f)$ if $\mathbf{S}_{xy}(f)$ and $\mathbf{S}_{xx}(f)$ have been measured or are known. This is of course a system of q simultaneous linear equations whose solution is

$$\mathbf{H}(f)=\mathbf{S}_{xx}^{-1}(f)\mathbf{S}_{xy}(f) \qquad (26)$$

Copyright © 1998, by the International Council of the Aeronautical Sciences (ICAS)
and the American Institute of Aeronautics and Astronautics, Inc.

where $\mathbf{S}_{xx}^{-1}(f)$ represents the inverse matrix to $\mathbf{S}_{xx}(f)$. Equation (26) gives each $H_i(f)$ as a function of the input/output cross-spectra $\mathbf{S}_{ij}(f)$, and holds whether or not the various inputs are correlated.

7.3 Multiple coherence functions

When computing the frequency response functions $\mathbf{H}(f)$ from the system of simultaneous equations defined in Equation (24), it is important to have some measure of the accuracy of the proposed model of the behaviour of the dynamical system that is being analysed. To this end, the multiple coherence function, which is a direct extension of the concept of ordinary coherence, provides a measure of the linear dependence between a collection of q inputs and an output, independent of the correlation among the inputs (Reference 8).

Referring to Figure 5, and following closely the theory presented in Reference 8, the multiple coherence function $\gamma_{y:x}^2$ between the output $y(t)$ and all the inputs $x_i(t)$, $i = 1, 2,\ldots, q$, that produce $y(t)$ is defined as the ratio of the ideal predicted linear output spectrum S_{vv} to the total measured output spectrum S_{yy},

$$\gamma_{y:x}^2 = \frac{S_{vv}}{S_{yy}} \tag{27}$$

Thus if

$$S_{yy} = S_{vv} + S_{nn} \tag{28}$$

where S_{nn} is the extraneous noise output spectrum, it follows that

$$\gamma_{y:x}^2 = \frac{S_{vv}}{S_{yy}} = \frac{S_{yy} - S_{vv}}{S_{yy}} = 1 - \frac{S_{nn}}{S_{yy}} \tag{29}$$

The notation $y:x$ means that portion of the output process $y(t)$ which is due to all the input processes $x_1(t), x_2(t),\ldots, x_q(t)$. From Equations (8) and (9), the general form of S_{vv} is

$$S_{vv} = \sum_{i=1}^{q}\sum_{j=1}^{q} H_i^* H_j S_{ij} = \sum_{i=1}^{q} H_i^* S_{iy} \tag{30}$$

Since $S_{vv} \le S_{yy}$, $S_{nn} \le S_{yy}$, and all terms are nonnegative, it follows for all frequencies f that

$$0 \le \gamma_{y:x}^2 \le 1 \tag{31}$$

If $\gamma_{y:x}^2(f) = 1$ then the model of the system behaviour is ideal and fully describes the relationship between the multiple inputs and the output. In actual practice, when the multiple coherence function is greater than zero but less than unity, one or more of the following four main conditions exist (Reference 8):

1. Extraneous noise is present in the measurements.
2. Resolution bias errors are present in the spectral estimates.
3. The system relating $y(t)$ to the $x_i(t)$ is not linear.
4. The output $y(t)$ is due to other inputs besides the $x_i(t)$ that are being considered.

From Equation (29), the product of the multiple coherence function and the output spectrum yields

$$\gamma_{y:x}^2 S_{yy} = S_{vv} = S_{yy} - S_{nn} \tag{32}$$

This product, called the multiple coherent output power spectrum, is a direct extension of the ordinary coherent output power spectrum for a single-input single-output system. It represents the fractional portion of the output spectrum S_{yy} due to all of the measured inputs $x_i(t)$, $i = 1, 2,\ldots, q$, that produce $y(t)$.

The output noise spectrum S_{nn} not due to any of the $x_i(t)$ is given here by

$$S_{nn} = \left(1 - \gamma_{y:x}^2\right) S_{yy} \tag{33}$$

Applications of these quantities requires that the input noise be negligible compared to the input signals, and that all of the input and output records be measured using a common time base so as to preserve their proper relative phase relationships.

In matrix notation, the multiple coherence function $\gamma_{y:x}^2$ can be expressed as

$$\gamma_{y:x}^2 = \frac{\mathbf{H}^{*T}\mathbf{S}_{xx}\mathbf{H}}{S_{yy}} \tag{34}$$

7.4 Solving the system of response equations

The basic underlying aim of the theory presented in Sections 7.1 and 7.2 is to develop a means for estimating the set of frequency response functions $\mathbf{H}(f)$. In its general form, the solution of Equation (26) will often

Copyright © 1998, by the International Council of the Aeronautical Sciences (ICAS)
and the American Institute of Aeronautics and Astronautics, Inc.

provide the answer. However, in the case where one or more of the inputs can be expressed as a linear combination of the remaining inputs, the inverse of the matrix $\mathbf{S}_{xx}(f)$ does not exist and the matrix $\mathbf{S}_{xx}(f)$ is classed as being singular. However, the possible singularity of $\mathbf{S}_{xx}(f)$ does not invalidate the equation, but simply poses additional problems in determining a meaningful solution.

Consider the familiar set of simultaneous equations

$$\mathbf{Ax} = \mathbf{b} \tag{35}$$

where $\mathbf{A}$ is a general complex square matrix and $\mathbf{x}$ and $\mathbf{b}$ are vectors. There exists a powerful set of techniques, called singular value decomposition (SVD), for dealing with sets of equations that are either singular or numerically very close to singular (Reference 10). SVD methods are based on the theorem of linear algebra that states that any general $N \times N$ complex matrix $\mathbf{A}$ can be written as the product of an $N \times N$ matrix $\mathbf{U}$, an $N \times N$ diagonal matrix $\mathbf{W}$ with positive real or zero elements w_i, and the conjugate transpose of an $N \times N$ matrix $\mathbf{V}$. This can be written as

$$\mathbf{A} = \mathbf{UWV}^{*T} \tag{36}$$

The w_i are the singular values of $\mathbf{A}$, such that $w_1 \geq w_2 \geq \ldots \geq w_q \geq 0$, and the columns of $\mathbf{U}$ and $\mathbf{V}$ are the left and right singular vectors of $\mathbf{A}$. The singular values and singular vectors satisfy

$$\mathbf{A}^{*T}\mathbf{u}_i = w_i\mathbf{v}_i \tag{37}$$

where the $\mathbf{u}_i$ and $\mathbf{v}_i$ are the ith columns of $\mathbf{U}$ and $\mathbf{V}$, respectively, and correspond to each of the w_i.

The matrices $\mathbf{U}$ and $\mathbf{V}$ are unitary, so their inverses are equal to their conjugate transposes, as expressed in the following equation

$$\mathbf{UU}^{*T} = \mathbf{VV}^{*T} = \mathbf{1} \tag{38}$$

$\mathbf{W}$ is a diagonal matrix, so its inverse is the diagonal matrix whose elements are reciprocals of the elements w_i.

From Equation (36) it now follows immediately that the inverse of $\mathbf{A}$ is

$$\mathbf{A}^{-1} = \mathbf{U}^{*T}\left[\text{diag}\left(\frac{1}{w_i}\right)\right]\mathbf{V} \tag{39}$$

If the matrix $\mathbf{A}$ is singular, one or more of the w_i's will be zero. When compared to the largest w_i, the smallest singular values are a good measure of whether the given matrix is singular. The condition number of a matrix is defined as the ratio of the largest (in magnitude) of the w_i's to the smallest w_i. A matrix is singular if its condition number is infinite, and it is ill-conditioned if its condition number is too large (that is, if its reciprocal approaches the computer's floating-point precision).

Substituting Equation (39) into matrix Equation (35), the SVD solution to the equation is computed using

$$\mathbf{x} = \mathbf{U}^{*T}\left[\text{diag}\left(\frac{1}{w_i}\right)\right]\mathbf{V}\,\mathbf{b} \tag{40}$$

where any of the terms $1/w_i$ in which the particular value of w_i is zero or very small are replaced by zero. It is necessary to exercise some discretion in deciding at what threshold to zero the small w_i's.

Turning now to the original cross-spectral matrix of the inputs $\mathbf{S}_{xx}(f)$, since it is Hermitian it has exactly q eigenvectors $\mathbf{r}_k$, which can be taken to be orthonormal, corresponding to the set of q real eigenvalues $\beta_1(f) \geq \ldots \geq \beta_q(f)$. This is expressed by

$$\mathbf{S}_{xx}\mathbf{r}_k = \beta_k\mathbf{r}_k \qquad k = 1, 2, \ldots, q \tag{41}$$

where the kth eigenvector is defined as having q components

$$\mathbf{r}_k(f) = \begin{bmatrix} r_{1k}(f) \\ \vdots \\ r_{qk}(f) \end{bmatrix} \tag{42}$$

These eigenvectors $\mathbf{r}_k$, $k = 1, 2, \ldots, q$, can be arranged columnwise into a square matrix $\mathbf{R}(f)$

$$\mathbf{R}(f) = \begin{bmatrix} r_{11}(f) & r_{12}(f) & \cdots & r_{1q}(f) \\ r_{21}(f) & r_{22}(f) & \cdots & r_{2q}(f) \\ \vdots & \vdots & \ddots & \vdots \\ r_{q1}(f) & r_{q2}(f) & \cdots & r_{qq}(f) \end{bmatrix} \tag{43}$$

Since $\mathbf{S}_{xx}(f)$ is also positive semi-definite, the eigenvalues β_k are known to have non-negative values. The spectral decomposition of $\mathbf{S}_{xx}(f)$ is then defined as

Copyright © 1998, by the International Council of the Aeronautical Sciences (ICAS)
and the American Institute of Aeronautics and Astronautics, Inc.

$$\begin{aligned}\mathbf{S}_{xx} &= \sum_{k=1}^{q} \beta_k \mathbf{r}_k \mathbf{r}_k^{*T} \\ &= \mathbf{R}\left[\mathrm{diag}(\beta_k)\right]\mathbf{R}^{*T} \\ &= \mathbf{U}\mathbf{W}\mathbf{V}^{*T}\end{aligned} \qquad (44)$$

The number of independent input signals can be determined from the multiplicity of the smallest eigenvalue of $\mathbf{S}_{xx}(f)$. In practice, however, the computed eigenvalues of $\mathbf{S}_{xx}(f)$ are all different because of the finite sample size.

It is evident in Equation (44) that the matrix form of the expression involving the eigenvalues and eigenvectors of $\mathbf{S}_{xx}(f)$ is in the general form defined for the SVD of $\mathbf{S}_{xx}(f)$. In this particular instance we have that $\mathbf{U} = \mathbf{V} = \mathbf{R}$. Therefore, after determining the spectral decomposition of $\mathbf{S}_{xx}(f)$ it is possible to apply the SVD technique to obtain the solution for the frequency response functions $\mathbf{H}(f)$ using the following equation

$$\mathbf{H}(f) = \mathbf{R}^{*T}(f)\left[\mathrm{diag}\left(\frac{1}{\beta_k(f)}\right)\right]\mathbf{R}(f)\mathbf{S}_{xy}(f) \qquad (45)$$

Having determined $\mathbf{H}(f)$ it is now possible to use this result to predict the autospectrum of $y(t)$ for any new set of inputs $x_1(t), x_2(t), \ldots, x_q(t)$ by using Equation (22). Here the output $y(t)$ can correspond to any chosen DLVC, while all the inputs $x_i(t)$ correspond to the set of control accelerometers.

7.5 TWDB development using multi-input predictions

Using the process shown in Figure 4, predicted DLVC rms response values per frequency band were computed from the control accelerometers. Flight test time histories for all DLVCs that had been bandpass filtered into the 10–20 Hz and 32–52 Hz bandwidths were scaled to match the predicted DLVC rms response targets. This was carried out for each AOA-Q bin and produced time histories which matched the target rms response level but whose response amplitude distributions corresponded to those that had been measured in flight. When combined with the pre-LEX fence usage data, target exceedence curves were produced which were used for comparison with the measured FT46 dynamic response. This collection of exceedence curves and the tables of rms response per AOA-Q bin constitute the IFOSTP Pre-LEX Fence Dynamic Response Database. A similar process will be undertaken using post-LEX fence flight trials data for use during the post-LEX fence phase of FT46 testing.

8. Analysis Of Test Results

At the completion of each test block the results are analysed to assess dynamic loading similarity between the test article and the flight test aircraft and that all measurands are functioning correctly. The analysis is performed using in-house software, which has been developed to handle the large amount of data collected and the binning of the data into AOA and Q bins. The software performs both time domain and spectral domain analyses.

The data are typically analysed for the set DLVCs for which flight test measurements are available for comparison with the measured FT46 results. Unless otherwise stated, results presented herein are for the fifth and final pre-LEX fence test block.

From a dynamics standpoint, only the buffet data are analysed, i.e. the data which represent flight conditions above 10° angle-of-attack. The effect of manoeuvre loading is only considered when looking at fatigue/life estimate calculations and will not be discussed here.

8.1 Time history results

The acceleration and strain data are primarily analysed in the time domain, as it is the time domain results which are more important from a fatigue standpoint. From this time domain analysis, tables of rms response levels, maximums, minimums and other statistics are obtained. Also obtained are exceedence curves. These data are then presented graphically, and compared to the targets that were obtained from the TWDB.

8.1.1 Accelerometer response

The primary accelerometers of interest are the four control accelerometers, mounted on the aft tip of each of the four primary flight control surfaces. There are also accelerometers mounted on the forward tips and on the engines which are also analysed to understand and monitor the dynamic response of the structure.

Tip response ratios are examined to give an indication of how correctly the modes are being excited during testing. Table 5 gives the tip response ratios for FT46, along with tip response ratios from the TWDB for comparison. From these results it can be seen that the FT46 and TWDB vertical tail and stabilator Mode 1 and vertical tail Mode 2 results are similar. However, for the stabilator Mode 2 response there is a significant difference between FT46 results and the TWDB. This difference is due to the incorrect combination of stabilator 2nd bending and 1st torsion modes and the reduction in stabilator loading in Mode 2 during pre-LEX fence testing. From the results in Table 5, it can also be seen that left-to-right the structure is reasonably symmetric, with the difference observed in

Copyright © 1998, by the International Council of the Aeronautical Sciences (ICAS)
and the American Institute of Aeronautics and Astronautics, Inc.

Table 5 – Tip response ratios (aft tip/fwd tip).

	FT46		TWDB*	
	Mode 1	Mode 2	Mode 1	Mode 2
Port Vert. Tail	1.68	2.21	1.78	2.09
Stbd Vert. Tail	1.71	2.30	2.13	1.99
Port Horiz. Stabilator	1.34	1.41	1.40	3.45
Stbd Horiz. Stabilator	1.31	1.56	1.28	4.10

*Note: TWDB tip response ratios are based on the predicted TWDB forward tip acceleration.

FT46 being replicated in the TWDB results, which are more representative of flight loading.

To see how well the FT46 response compares with the TWDB targets, exceedence curves are prepared for all the DLVCs. Exceedence curves for the vertical tail first bending and first torsion modes are presented in Figure 6 and Figure 7, respectively. These exceedence curves show that the amplitude distribution of the response measured on FT46 is similar to the response of the TWDB. There are some slight differences left-to-right, but these differences are also observed when the flight data are compared left-to-right. Note that the target that is presented is a combined left-right target.

Similar curves to these are also prepared for the stabilator and engine accelerations; however, they are not presented here.

8.1.2 Strain gauge response

As the primary aim of IFOSTP is to determine the fatigue life of the F/A-18 structure, the response at the strain gauges is also assessed against the flight test data. When assessing strain gauge results, it must be kept in mind that the test is controlled on acceleration, and it is assumed that if the target accelerations are met, and the modes are similar to those of a fleet aircraft, the strains measured on the test article will also be representative of strain present on fleet aircraft. However, several points must be considered when comparing FT46 and flight strains. Firstly, slight differences in gauge placement in high stress gradient regions can significantly affect the strain measurement. Also, structural differences between FT46 and flight test aircraft will likely cause differences in strain response. However, this is difficult to quantify as no static or dynamic calibrations were performed on the flight test aircraft.

The strain gauge response will be discussed in relation to the four primary structural regions with which the IFOSTP test is concerned, namely the vertical tail attachment

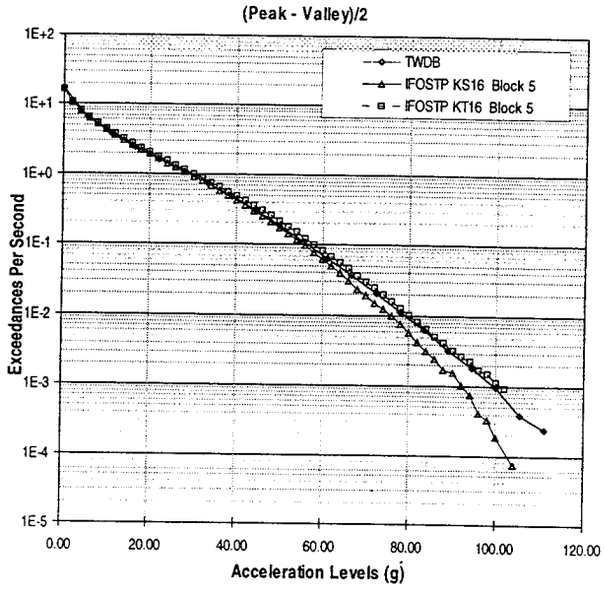

Figure 6 – Vertical tail first bending mode exceedence curve.

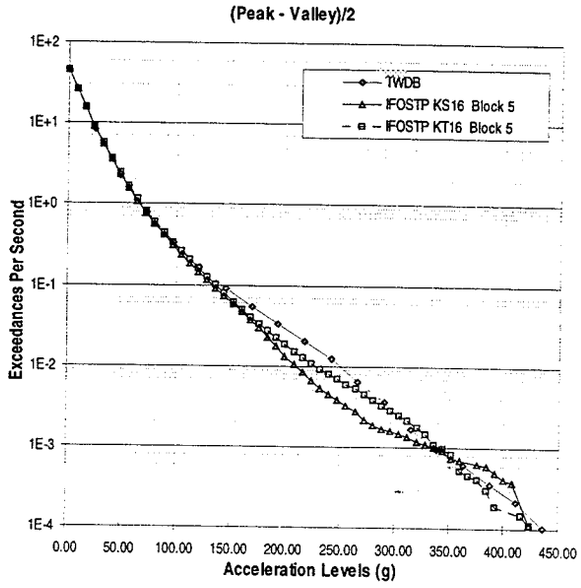

Figure 7 – Vertical tail first torsion mode exceedence curve.

fittings, the stabilator support structure, the fuselage and the engine mounts.

8.1.2.1 Vertical tail strain gauge response

Vertical tail strain gauges on the DLVC list are installed on the vertical tail fuselage attachment stub frames. For these locations it is possible to obtain a strain/g distribution, which can then be compared to flight test. Figure 8 and Figure 9 show the strain/g distribution at the vertical tail to fuselage interface for vertical tail modes 1 and 2, respectively, compared to the results obtained from the AETE PD 88/12 flight test program. To illustrate the slight change which the structure has undergone during the

Copyright © 1998, by the International Council of the Aeronautical Sciences (ICAS)
and the American Institute of Aeronautics and Astronautics, Inc.

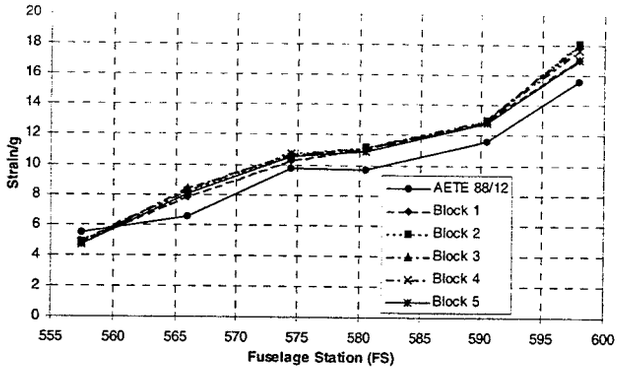

Figure 8 – Vertical tail stub strain/g for first bending.

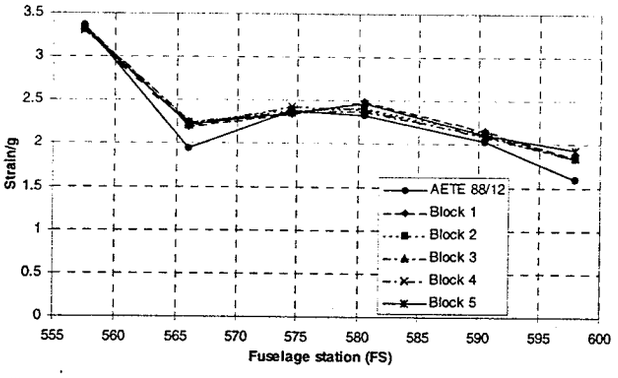

Figure 9 – Vertical tail stub strain/g for first torsion.

pre-LEX fence testing stage, all five blocks of pre-LEX fence testing are shown in these two figures. As can be seen from these results, the distribution of strains at the root of the vertical tail is comparable to the distribution obtained during flight testing. This indicates that the vertical tail modes are behaving as expected under the applied loading.

8.1.2.2 Stabilator strain gauge response

For the stabilators, the DLVC strain gauges are located on the stabilator spindle attachment blocks, one gauge per side. The strain/g figures for both sides from FT46 are presented in Table 6, where it can be seen that there are significant differences in both bands between the TWDB and FT46 results. These differences are due to two primary effects.

For Mode 1, indications are that the strain response at the spindle block is influenced by a fuselage mode as well as stabilator bending. As the IFOSTP test is not set up to control the fuselage modes, which are different to a fleet aircraft because of the manner in which the test article is mounted minus wings in the test rig, the fuselage component of the strain will be different to that of a fleet aircraft. Thus the only component of strain that can be achieved with the given test approach is that associated with stabilator first bending. This is deemed to not have a significant effect on the test as a whole, as it has been found that the majority of the fatigue damage at the spindle

Table 6 – Strain/g values for stabilator.

	FT46 (Block 4)		TWDB*	
	Mode 1	Mode 2	Mode 1	Mode 2
Port	4.79	1.19	8.94	1.95
Starboard	4.49	1.20	9.15	2.33

*Note: TWDB response values are based on the predicted TWDB forward tip acceleration.

block is caused by the manoeuvre loading rather than the dynamic/buffet loading.

The difference in the strain/g for the second bandwidth is likely caused by the unrepresentative combination of stabilator 2nd bending and 1st torsion.

8.1.2.3 Fuselage strain gauge response

There are four DLVC fuselage strain gauges. Three of these gauges are installed on the FS598 bulkhead, with the fourth installed on the upper longeron at FS557. These gauges are not well correlated with the control accelerometers, and as such the measured results are not expected to match up well with the TWDB results. Two of the three gauges installed on the bulkhead are lower than the TWDB targets in the first bandwidth, with one being higher. For the second bandwidth, one gauge is low, with the other two being high. The fourth gauge, installed in the upper longeron, is lower for both bandwidths when compared to the TWDB. The difference observed in the fuselage strains between FT46 and the TWDB has been deemed to be not significant enough to halt testing due to the aforementioned low correlation with the four control accelerometers. However, these differences will have to be addressed when assessing test results.

8.1.2.4 Engine mount strain gauge response

For the pre-LEX fence stage of testing, only one strain gauge is installed on FT46 for which there is a comparable flight test gauge. It is mounted on the port aft engine hanger. As has been previously mentioned, there have been some problems getting the engine loading correct, which has influenced the results obtained in the testing completed to this stage. For Mode 1, the engine strains are slightly lower than target. However, for the Mode 2 region the measured strains are significantly different than those specified in the TWDB. This is consistent with the low stabilator loading in the second bandwidth. A definitive statement on the engine strain results cannot be made until the development work for the post-LEX fence stage of testing has been completed.

8.2 Spectral results

As previously mentioned, the majority of the FT46 data analysis is performed in the time domain. The cyclic nature of the dynamic loading is important in fatigue testing, and

Copyright © 1998, by the International Council of the Aeronautical Sciences (ICAS)
and the American Institute of Aeronautics and Astronautics, Inc.

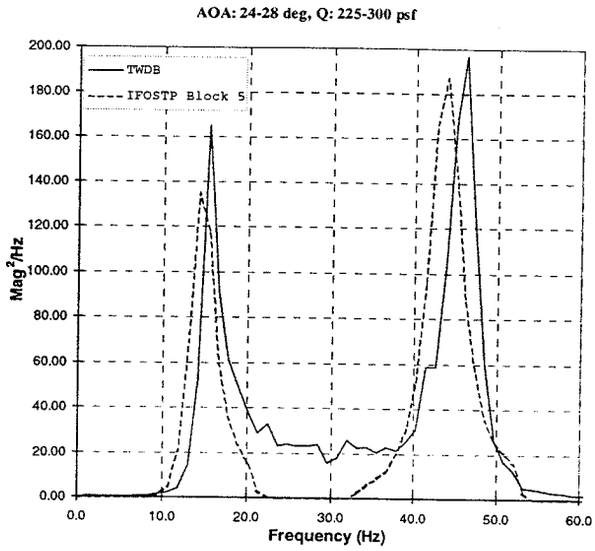

Figure 10 – PSD for KS16.

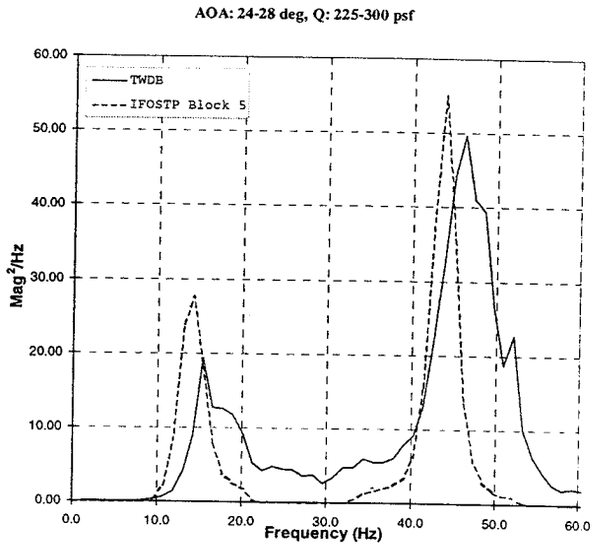

Figure 11 – PSD for KQ64.

time constraints means the time domain analysis is given a higher priority for FT46. However, at the completion of each test block a spectral analysis is performed on the data to produce power spectra and frequency response functions. Typically, the data are processed using FFT techniques, with a 512 sample block size and a Hanning window applied to the data. A primary use of the spectral domain data which are gathered is for use in strain predictions.

As it is possible to only monitor a certain number of channels at any one time, a technique has been developed whereby the strains at unmonitored locations can be predicted through the use of strain/acceleration frequency response functions and the PSDs of the four control accelerometers. By using an inverse FFT procedure, each predicted strain response PSD can be converted to a predicted time-domain strain sequence which can then be used in fatigue damage calculations (Reference 11).

8.2.1 Accelerometer response

Power spectra for the four FT46 control accelerometers can be compared to power spectra obtained from flight test aircraft. An example of a power spectrum for the accelerometer mounted on the aft tip of the port vertical tail is shown in Figure 10. The PSD plots shown in this figure are for one AOA-Q bin, which was chosen to be indicative of the trends observed in the FT46 and flight test data, showing reasonable response in both excitation bands. This plot shows that the test article and flight test aircraft have a similar spectral response, in terms of shape and magnitude, however the resonance occurs at a slightly lower frequency on the test article than was observed in flight. A similar variation has also been seen amongst the data acquired from other flight tests. Also, there is very little response between the bands for the test article response, which is to be expected as there is no input excitation applied here.

Figure 11 shows the PSD for the port stabilator aft tip accelerometer. As can be seen from this plot, there is some difference in the spectral content of the test article and the flight test aircraft. This is partly to be expected due to the problems encountered with the stabilator loading, particularly in the second bandwidth. This plot also illustrates the way in which the two FT46 modes present in the second bandwidth combine in a way which differs from that which occurs in flight. It should also be noted that there is some difference in the shape of the PSDs for Mode 1, however the energy content between flight test aircraft and the test article are similar, as indicated by similar rms response values. The Mode 2 energy content is slightly different, due to the previously mentioned problems with the shaker location.

9. Post-LEX Fence Dynamic Loading Issues

From results obtained prior to and during pre-LEX fence testing, several areas are of particular interest and concern for future post-LEX fence testing.

Firstly, as discussed in a previous section, the stabilator shaker has been relocated from the pre-LEX fence trailing edge location to a leading edge location. This new shaker location will be evaluated and full stabilator excitation will be applied for the first time during post-LEX fence testing. This additional 34–52 Hz excitation will be evaluated at critical stabilator reaction points and is also expected to have a significant impact on engine dynamic loading.

Engine dynamic loading is of critical importance during post-LEX fence testing. After pre-LEX fence testing was completed, new engine mounts and backup structure were

Copyright © 1998, by the International Council of the Aeronautical Sciences (ICAS)
and the American Institute of Aeronautics and Astronautics, Inc.

incorporated into the airframe as part of a planned retrofit that had been incorporated into all fleet aircraft at approximately the time of installation of the LEX fence. Thus, the impact of any incorrect engine loading during pre-LEX fence testing was not as critical as it will be during post-LEX fence testing. For this reason, the engine dynamic loading is currently being studied. Additionally, in order to more adequately define the engine loading, a significant amount of post-LEX fence flight test data was acquired for this new engine mount configuration, providing strains at the aft hanger engine mounts and at 15 strain gauges installed on the forward engine mounts.

As part of the investigation into engine dynamic response and engine mount loading, additional accelerometers have been installed FT46 to measure the dynamic response of the fuselage. It is believed that fuselage motion may be a large contributor to the engine mount dynamic loading. However, as flight test data are not yet available to quantify the in-flight aft fuselage vibration, plans are in place to try to obtain flight test accelerations for the engines and aft fuselage, as well as the empennage surfaces. This data can then be compared to that acquired during IFOSTP FT46 testing.

These issues, as well as the validation of post-LEX fence empennage dynamic loading, will be investigated as part of the validation of the first block of post-LEX fence dynamic loading.

10. Conclusion

AMRL has completed the pre-LEX fence phase of the fatigue testing of the F/A-18 aft fuselage and empennage. This test represents a significant milestone in the history of full-scale fatigue testing of aircraft structures. The AMRL test is unique in that it is the first time that realistic dynamic buffet loads and manoeuvre loads representative of those encountered in actual flight are applied simultaneously. This testing method has the significant advantage that the high-frequency dynamic loads can be applied in real time, keeping the test duration for buffet loading to a minimum. The test results available to date indicate that the dynamic testing approach is a viable one. Preparations are now proceeding for the post-LEX fence phase of FT46 testing, where further assessment and fine tuning of the approach will take place.

11. Acknowledgments

The authors wish to thank their colleagues at AMRL who have contributed to the large team effort required for a test of this magnitude and complexity.

12. References

1. D.P. Conser, A.D. Graham, C.J. Smith and C.L. Yule, *The Application of Dynamic Loads to a Full-Scale F/A-18 Fatigue Test Article*, ICAS Proceedings 1996, Volume 2, Paper ICAS-96-5.10.5, pp. 2465–2480, 20th Congress of the International Council of the Aeronautical Sciences, Sorrento, Napoli, Italy, 8–13 September, 1996, ISBN 1-56347-219-8.

2. N.H. Zimmerman and M.A. Ferman, *Prediction of Tail Buffet Loads for Design Application*, McDonnell Aircraft Company, St. Louis, Missouri, Report No. NADC-88043-60, July 1987.

3. D.H. Thompson, *Effect of the Leading-Edge Extension (LEX) Fence on the Vortex Structure Over the F/A-18*, DSTO Technical Report DSTO-TR-0489, Air Operations Division, Aeronautical and Maritime Research Laboratory, February 1997.

4. M.G.J. Higgs and A.S. Currie, *Development of the F/A-18 Usage Spectrum for the FT46 Fatigue Test – Pre-LEX Fence Flying*, DSTO Technical Report DSTO-TR-0393, Airframes and Engines Division, Aeronautical and Maritime Research Laboratory, September 1996.

5. K.K. Streber and J.P.L. Rioux, *CF-188 Aft Fuselage Strain and Vibration Survey*, AETE Project Report 88/12, Canadian Forces, Aerospace and Engineering Test Establishment, 6 May 1992.

6. N. Landry, *CF-188 Horizontal Stabilizer/Engine Hanger Dynamic Strain Measurements in Flight*, AETE Project Report 93/03, Canadian Forces, Aerospace and Engineering Test Establishment, 15 March 1996.

7. W. Waldman, *Design and Implementation of Digital Filters for Analysis of F/A-18 Flight Test Data*, Aircraft Structures Technical Memorandum 555, Aeronautical Research Laboratory, May 1992.

8. J.S. Bendat and A.G. Piersol, Engineering Applications of Correlation and Spectral Analysis, 2nd Edition, John Wiley & Sons, Inc., 1993, ISBN 0-471-57055-9.

9. J.S. Bendat and A.G. Piersol, Random Data: Analysis and Measurement Procedures, 1st Edition, John Wiley & Sons, Inc., 1971, ISBN 0-471-06470-X.

10. W.H. Press, B.P. Flannery, S.A. Teukolsky and W.T. Vetterling, Numerical Recipes in C – The Art of Scientific Computing, 2nd Edition, Cambridge University Press, 1993, ISBN 0-521-43108-5.

Copyright © 1998, by the International Council of the Aeronautical Sciences (ICAS)
and the American Institute of Aeronautics and Astronautics, Inc.

11. W. Waldman, *Development of F/A-18 Buffet Response Strain Sequences for Use in Fatigue Damage Calculations and Coupon Testing*, DSTO Technical Report DSTO-TR-0365, Airframes and Engines Division, Aeronautical and Maritime Research Laboratory, July 1996.